Article

Effect of Different Acoustic Parameters on NOx Emissions of Partially Premixed Flame

Kai Deng [ID]**, Mingxiao Wang** [ID]**, Zhongliang Shen, Yanjun Hu and Yingjie Zhong *** [ID]

Institute of Energy and Power Engineering, Zhejiang University of Technology, Hangzhou 310014, China; dkai@zjut.edu.cn (K.D.); wmxgood@126.com (M.W.); superman_panda@163.com (Z.S.); huyanjun@zjut.edu.cn (Y.H.)

* Correspondence: zhong_yingjie@zjut.edu.cn; Tel.: +86-0571-88320650

check for updates

Featured Application: The results of the research can be used in the design of low NOx pulsating burners to determine the corresponding frequency and amplitude.

Abstract: The effects of acoustic frequency (f)/0–400 Hz and amplitude (A)/0–1400 Pa on nitrogen oxides (NOx) emissions of a partially premixed flame were investigated experimentally. The mechanism of NOx emissions was analyzed by the evolution of the vortex, which was shown by particle image velocimetry (PIV). From the relationship of NOx emission index (EINOx) and acoustic parameters, it was concluded that a critical frequency (f_c) from 170 Hz to 190 Hz appeared. When the frequency was less than f_c, EINOx decreased linearly with an increase in amplitude. The flame length became shorter, which led to a decrease in the global residence time, and hence, a reduction in reaction time for NOx. However, a direct proportional relationship between EINOx and amplitude was not found when the frequency was larger than f_c. Based on PIV particle scattering images, with an increase of the acoustic frequency, the effects of the acoustic field on the flame base became less significant, but the flame length and reaction space of NOx were gradually increased.

Keywords: acoustic; frequency; NOx emission index; flame length; global residence time

1. Introduction

There is a growing interest in alternative technologies for energy generation applications, which can range from the emerging of hybrid solar receiver–combustor (HRC) technologies [1,2] to simpler fuel blending approaches, such as the co-firing of biomass feed stocks with coal for power generation purposes [3,4], because of increasing pressure to conserve ever diminishing fossil fuel resources and to reduce pollutant emissions. Excessive emissions of nitrogen oxide (NOx) from power generation applications is a severe problem that can lead to increased occurrences of acid rain and photochemical smog pollution. This has also led to research and investment into low NOx combustion technology [5–7], such as pulsed combustion technology. Pulse combustion technology is one of the highly combustion efficient and low NOx combustion technologies that have been demonstrated in engineering application. Pulse/pulsating combustion refers to the unstable combustion process under the effects of sound field or pulsating flow, while the steady-state variables such as temperature, pressure, air velocity, and heat release rate fluctuate periodically with time in the combustion zone. This phenomenon about heat excited acoustic oscillations was firstly observed by Rijke, who discovered that strong acoustic oscillations occurred when a heated metallic grid was positioned in the lower half of a vertical tube opened at both ends [8]. Rayleigh stated that the sound could be excited in a closed volume only if the pressure oscillation is in phase with the heat-release oscillation [9]. Based on Rayleigh's criterion, different kinds of pulse combustors, including the Rijke, Hemholtz, Schmidt

pulse combustor, were developed and widely used in power and heat generation devices, including boilers, water heaters, industrial furnaces, and pulsating dryers for a long time [10–14].

Previous studies showed that the reductions in NOx could occur for lean premixed flames under acoustic excitation [13–17]. Lean premixed flames are more sensitive to flow perturbations and tend to induce self-excited thermoacoustic oscillations. However, in terms of NOx reduction, the effects of acoustic excitation on partially premixed flame and diffusion flame could potentially be more effective [18–21], as the lean premixed flame inherently has very low NOx emissions. Partially premixed flames have dual flame dynamics characteristic of lean premixed flame and diffusion flame. Therefore, it has engineering and academic value to investigate partially premixed flame, which is also widely used in boilers and industrial furnaces.

Understanding the characteristics of partially premixed combustion systems under acoustic excitation, in terms of NOx emissions, is still limited because the complexity involved in the interaction between upstream disturbances and reacting flow fields [22]. Kim et al. proposed that the reduction of flame length was the main reason for the decrease of the NOx emission index (EINOx), by investigating flames under acoustic frequencies of 256.9 Hz, 400 Hz, 770.6 Hz, and 514 Hz [23]. In conclusion, interaction between acoustic excitation and flame were demonstrated to lead to reduced NOx emission for premixed flame and diffusion flame [24,25], but the effects of acoustic parameters including frequency and amplitude on NOx emissions for partially premixed flame were rarely reported. Recently, Shen [26], Deng [27,28], and Zhong [29] focused on the NOx emission of partially premixed flame in Rijke tubes with an acoustic frequency of 110 Hz, and observed that the reduction of high temperature area and the decrease of residence time were major causes for NOx reduction. However, the exact relationships between amplitude, frequency, and EINOx have not been obtained. Present work focuses on the effects of acoustic frequency (0–400 Hz) and amplitude (0–1000 Pa) on NOx emissions with partially methane/air premixed flame. The correlation of the NOx emission results to the changes in flame properties, such as flame length, flame shape, and global residence time, in response to variations in the controlling parameters was analyzed.

2. Materials and Methods

2.1. Experimental Setup

The experimental system consisted of the combustor and a sound generating device, as seen in Figure 1. It is an atmospheric, partially premixed combustor, consisting of an annular jet burner with a coflow tube and an optically accessible quartz combustion chamber. The improved Burke–Schumann burner, which was referenced in Hassan et al. [21] and Illingworth et al. [30], was designed. This Bunsen burner was installed in the center of a coflow tube (1600 mm $\times$ Φ140 mm) with two rectangular-shaped quartz windows (90 mm $\times$ 400 mm). The burner had an inner diameter, d_F, of 18.0 mm and a lip thickness of 2.0 mm. The inner diameter of the coflow tube, d_C, was 150 mm. The coflow air jet was injected parallel to the central jet of the methane mixture to provide enough oxygen for the combustor. The coflow air was maintained at a sufficiently low velocity, less than 0.1 m/s, so as not to disturb the flow field in the combustion area. Porous medium plates were set in the coflow tube to ensure a uniform airflow. A loud speaker (A0208A, JBL, Northridge, CA, USA) with a signal generator (AFG-2225, GW-INSTEK, Taiwan, China) and amplifier (E-470, Accuphase, Yokohama, Japan) were placed at the bottom of the combustor as a forced acoustic source to provide adjustable acoustic frequencies and amplitudes (see Figure 1).
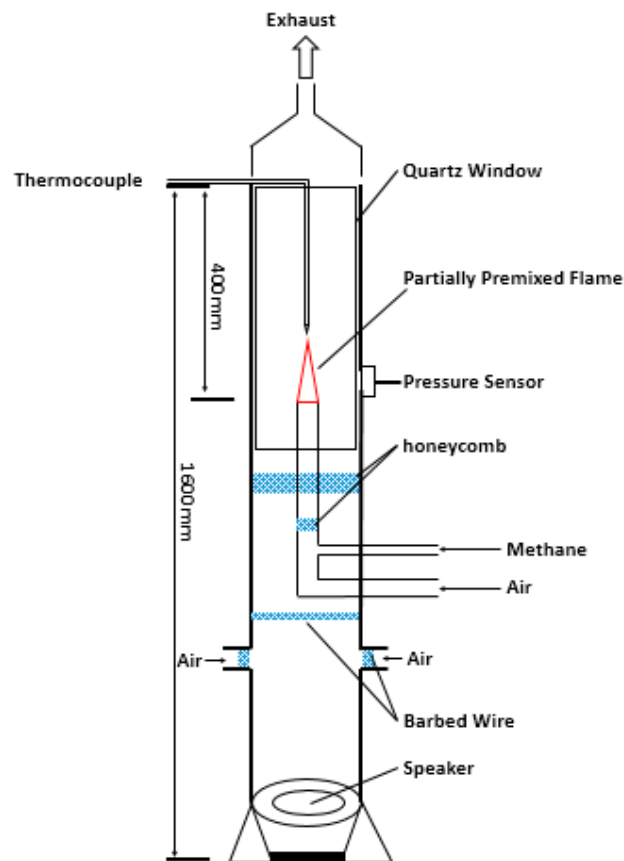
Figure 1. Experimental system.

2.2. Instrumentation and Acquisition

A pressure sensor (CYG1409T, Shuang Qiao, Kunshan, China), which was installed at the flame location and perpendicular to the cylinder's axis, was employed to measure the acoustic frequency and amplitude in the cylinder. The pressure sensor had a measuring range of 0–3000 Pa and a measuring accuracy of 1%. The results were obtained after fast Fourier transform (FFT) by a data acquisition system (PXI-1033, NI-DAQ).

As shown in Figure 2, the flame length was measured by processing the images taken by a high-speed digital camera (MVC1000DAF-GE1000, Microview, Beijing, China). A digital single-lens reflex (DSLR) camera (Canon, EOS 550d, Tokyo, Japan) was used to observe flame structures and flame surface wrinkling. The exposure time for the high-speed camera was set at 1/1000 s. To visualize the flow field, a particle image velocimetry (PIV) system (Dantec Dynamics, Copenhagen, Denmark) was utilized to describe the flame response under acoustic excitation. The PIV system consists of a YAG laser generator with double 200 mJ pulses at 532 nm and a Dantec Dynamics Flow Sense 4 M digital camera with 2048×2048 pixels. Al_2O_3 seeding particles about 2.5 μm in diameter were used to seed the coflow air tube.

A 2D cross-correlation FFT algorithm incorporating a multi-pass approach was used to analyze corresponding particle image pairs. The initial pass of the routine analyzed the images using 32 by 32 pixel interrogation regions, and the final pass used interrogation regions of 16 by 16 pixels. A 3-point Gaussian peak search algorithm was used to calculate sub-pixel displacement and a 50% Nyquist overlap of the regions was incorporated.

Phase-resolved PIV measurement was triggered by the signal from the pressure sensor. A compromise on the number of PIV image pairs was made for the phase-resolved PIV experiments. This was because the sampling rate was low due to phase jitter and a longer duration of the experiments would exacerbate the problem associated with deposition of seed particle on the enclosure wall. The

100 image pairs collected were deemed sufficient to produce stable mean velocities for examining the evolution of the flow field structures of partially premixed flame.
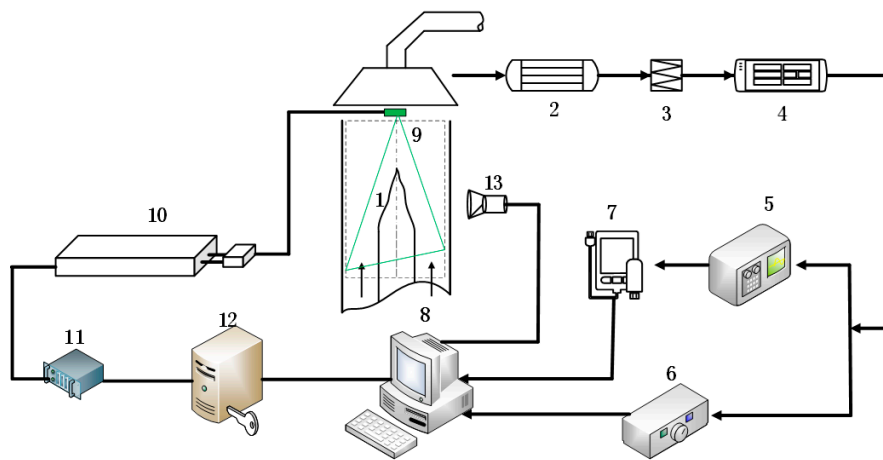
Figure 2. Schematic diagram of the experimental setup used for measurements (1. Flame; 2. Insulation pipe; 3. Filter; 4. Preprocessor; 5. Photon flue gas analyzer; 6. NOx Analyzer; 7. Data Acquisition; 8. Computer; 9. Laser; 10. Laser generator; 11. Synchronizer; 12. Controller; 13. Camera).

The flame length was obtained by flame area image processing [31–33]. The flame contour and flame length were obtained by selecting the threshold value in the flame area image, which was captured by high-speed camera. The average flame length was calculated based on every 2000 photos. An electrochemical NOx sensor (CLD64, ECO Physics, Duernten, Switzerland) was located after the flue gas collection device, and the collection device used was made with reference to Costa's work but with slight modifications for adapting the size of the combustor [34]. Another infrared fuel gas analyzer (Photon, Madur, Vienna, Austria) was used to measure components of the exhaust gas. Measurement precision of components are shown in Table 1.

Table 1. Measurement range and measurement accuracy of the gas analyzer for different gas components.

Component	Measurement Instrument	Measurement Range	Measurement Accuracy
O_2		0–25%	±0.2% or 2% rel
CO_2	MADUR PHOTON infrared gas	0–25%	±0.1% or 3% rel
CO	analyzer	0–20,000 ppm	±3 ppm or 3% rel
CH_4		0–5%	±0.1% or 3% rel
NO	ECO Physics CLD60	0–0.5 to 0–100 ppm	2 ppb
NO_2	electrochemical NOx analyzer	0–0.5 to 0–100 ppm	2 ppb

The NOx emission index (EINOx) was employed to characterize NOx emissions, which were defined as NOx per unit mass fuel. Assuming that all the carbons in the fuel are completely converted into CO_2 and CO, EINOx is defined as:

$$\text{EINOx} = \left(\frac{x_{NO_x}}{x_{CO} + x_{CO_2}}\right) \cdot \left(\frac{mMW_{NOx}}{MW_F}\right). \tag{1}$$

Here, x_i is the mole fraction, m is the number of carbon atoms in the fuel, and MW_i is molar mass.

According to the measurement error transfer formula, the arithmetic average error of EINOx is:

$$\Delta\text{EINOx} = \left(\frac{\Delta x_{Nox}}{x_{CO} + x_{CO_2}} + \left(-\frac{\Delta x_{CO} \cdot x_{Nox}}{(x_{CO} + x_{CO_2})^2}\right) + \left(-\frac{\Delta x_{CO_2} \cdot x_{Nox}}{(x_{CO} + x_{CO_2})^2}\right)\right)\left(\frac{xMW_{NOx}}{MW_F}\right). \tag{2}$$

The EINOx deviation was 0.001–0.005 g/kg, which was less than 1% of experimental values, which means the experimental data was accurate.

2.3. Experimental Conditions

The primary equivalence ratios (Φ) of 2 and 3 were selected for comparison because the partially premixed flame would not flash back or blow off under acoustic excitation at these equivalence ratios. Methane and air flow rates were controlled by the mass flow controller (Sheng Ye, SY-93) with precision of approximately 1%. Experimental conditions are summarized in Table 2.

Table 2. Experimental conditions.

Experimental Conditions	CH$_4$ (mL/min)	Air (mL/min)	Φ	Re	Coflow Air (mL/min)	f (Hz)	A (Pa)
Case 1	1000	5000	2	422.1			
Case 2	1500	5000	3	476.8	10,000	0–400	0–1400
Case 3	1500	7500	2	663.1			

The mean velocities of premixed fuel in the combustor were 0.393 m/s, 0.5895 m/s, and 0.426 m/s corresponding to case 1, case 2, and case 3, respectively. The average velocity of coflow air was 0.00964 m/s; therefore, the influence of the coflow air on the flame structures and flame surface wrinkling could be ignored. The Reynolds number ranged from 422.1 to 663.1, which belonged to laminar combustion without acoustic excitation. For laminar flame, the relationship between NOx and the flow field induced by acoustic excitation was more clearly. Comparison of NOx emission characteristics with equivalence ratios and Reynolds numbers were conducted.

The ranges of acoustic frequency and acoustic amplitude were selected between 0–400 Hz and 0–1400 Pa. Firstly, pulsed combustors tend to operate at low frequencies, usually around 100 Hz [17]. Secondly, based on the experimental results of the premixed flame under acoustic excitation, Bourehla [35] found the flame shape changed significantly within the frequency range of 100 Hz to 220 Hz. In addition, the flame structure also changed significantly following an increase in the amplitude. Furthermore, the acoustic response of the speaker had a good behavior between 0–400 Hz and 0–1400 Pa. The maximum of acoustic amplitude was 1400 Pa, and pressure amplitude p'_n could be converted to velocity amplitude u'_n by conversion relations [36,37]:

$$p'_n / u'_n = \rho_m c. \tag{3}$$

Herein n is acoustic mode; ρ_m is density (=0.946 kg/m^3); c is sonic speed (=387.23 m/s). As a result, the maximum of acoustic velocity amplitude was 3.8218 m/s.

2.4. Acoustic Characteristics of Experimental System

Acoustic amplitude and frequency were adjustable in this experiment. The measured results of 180 Hz with 579.04 Pa acoustic are shown in Figure 3; no obvious signal noise was apparant. Therefore, reliability of the acoustic excitation was verified.
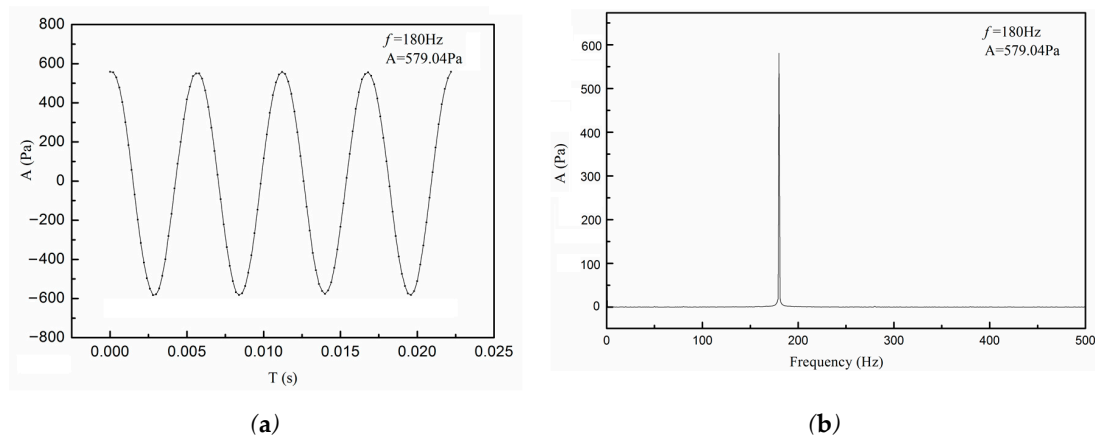
Figure 3. Acoustic pressure of the experimental system; (**a**) Time domain; (**b**) Frequency domain

3. Results and Discussion

3.1. The Relationship between EINOx with Acoustic Amplitude

The NOx emissions for partially premixed flame under acoustic excitation are plotted in Figure 4. The linear relationship between acoustic amplitude and EINOx were presented at a fixed frequency. Under three different premixed gas parameters, the lines displayed a negative slope when the frequency was less than 180 Hz, while a positive slope appeared when the frequency was more than 190 Hz. Therefore, a critical frequency (f_c) was defined between 170 Hz and 190 Hz, which was consistent with Delabroy's results from a liquid boiler [20].
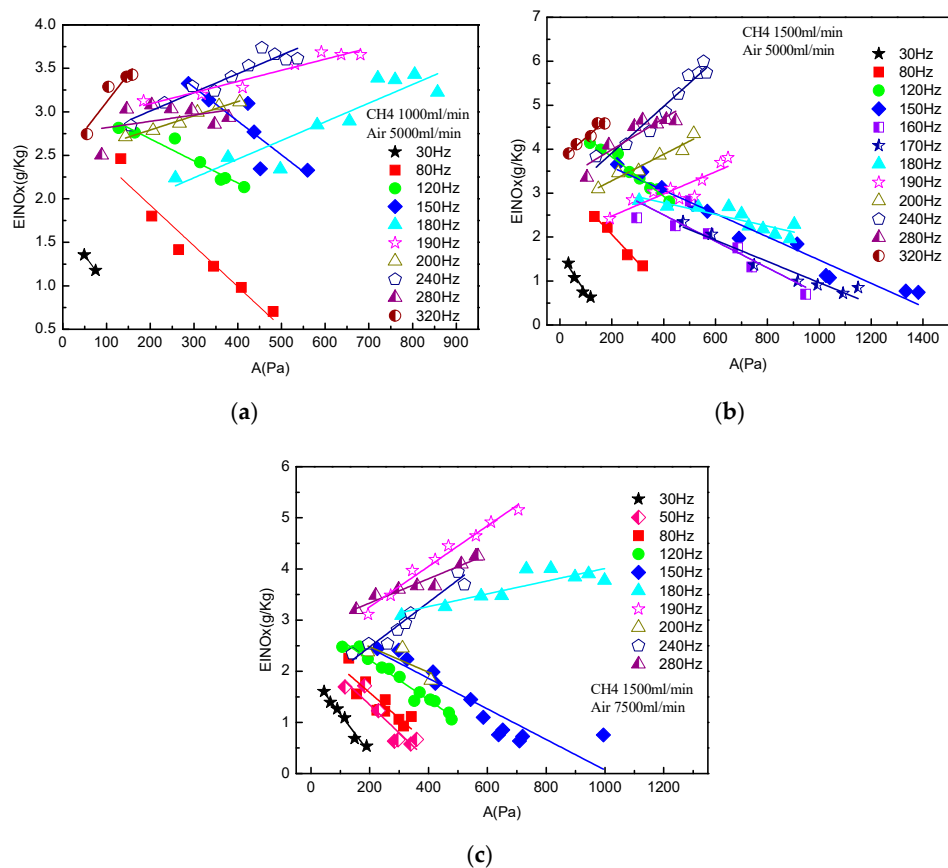

Figure 4. The relationship between acoustic parameters and NOx emission index (EINOx) for partially premixed flame; (**a**) Case 1; (**b**) Case 2; (**c**) Case 3.

EINOx and amplitude had linear relationships in each case. EINOx reduced 15% to 30% with the increase of amplitude by every 100 Pa when frequency was less than f_c. Furthermore, the slope in this region ranged from -0.009 to -0.003. In contrast, the linear relationships were reversed when the frequency was greater than f_c; the positive slopes were also observed to range from 0.001 to 0.006. In a word, EINOx decreased with the increase of acoustic amplitudes while frequency was less than f_c, and increased while the frequency was greater than f_c.

3.2. The Relationship between EINOx and Acoustic Frequency

The effects of acoustic frequency on NOx emissions are shown in Figure 5. There was a clear linear relationship between EINOx and frequency when frequency was less than f_c, as seen in Figure 5. The positive slope of the linear relationship between EINOx and acoustic frequency ranges from 0.001 to 0.003. However, the relationship between the frequency and EINOx is not clear when $f > f_c$. This is related to the flame response to acoustic excitation at different frequencies.
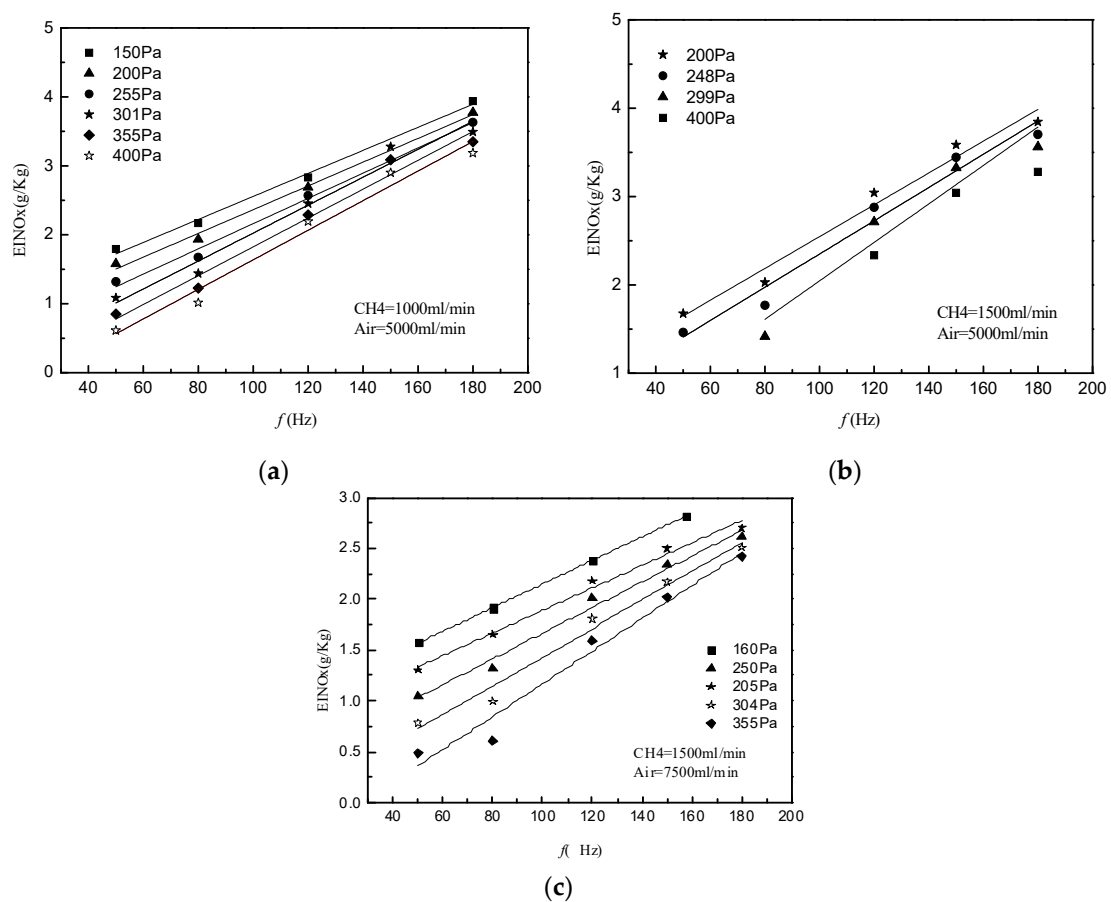
Figure 5. NOx emission characteristics with acoustic amplitudes (0–180 Hz) (**a**) Case 1; (**b**) Case 2; (**c**) Case 3.

3.3. Flame Length and Flame Surface Wrinkling

The flame images were taken by a Canon CMOS (Complementary Metal Oxide Semiconductor) camera to show the flame structures under the different frequencies. In Figure 6, the images are illustrated for case two of partially premixed flames with a range of acoustic frequency from 80 Hz to 280 Hz based on time-average images. Flame surface wrinkles were quite different with acoustic frequencies at a fixed acoustic amplitude of 345 ± 10 Pa. The effects of acoustic forcing on flame wrinkling at 80 Hz to 150 Hz were much stronger than 200 Hz to 280 Hz, which was in good agreement with the results in the change of NOx emissions with acoustic frequency.
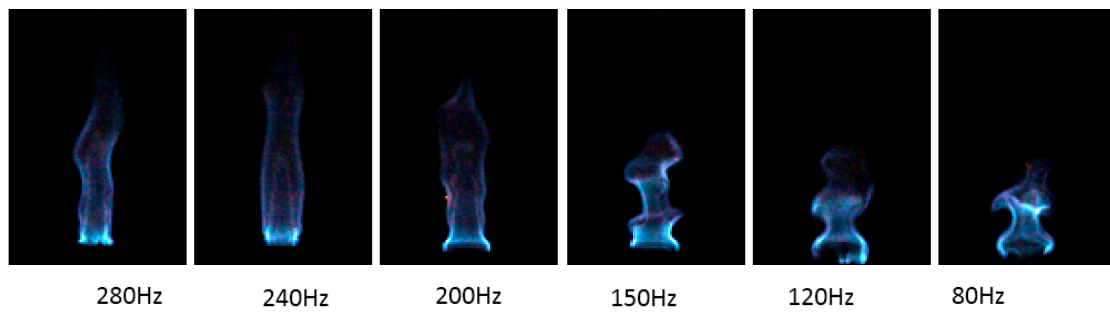
Figure 6. Flame surface wrinkling under different frequencies (345 ± 10 Pa).

Flame length (L_f) can quantitatively describe the relationship between acoustic parameters and EINOx for jet flame. Compared with Figures 4 and 7, this was consistent with the relationship between acoustic amplitude and NOx. Flame length decreased visibly with a gradually increase of acoustic amplitude when the frequency was less than 170 Hz. There was also a good linear correlation between the flame length and the acoustic amplitude when the frequency was less than 170 Hz. However, there was no obvious regularity between flame length and acoustic amplitude when the frequency was larger than 170 Hz.
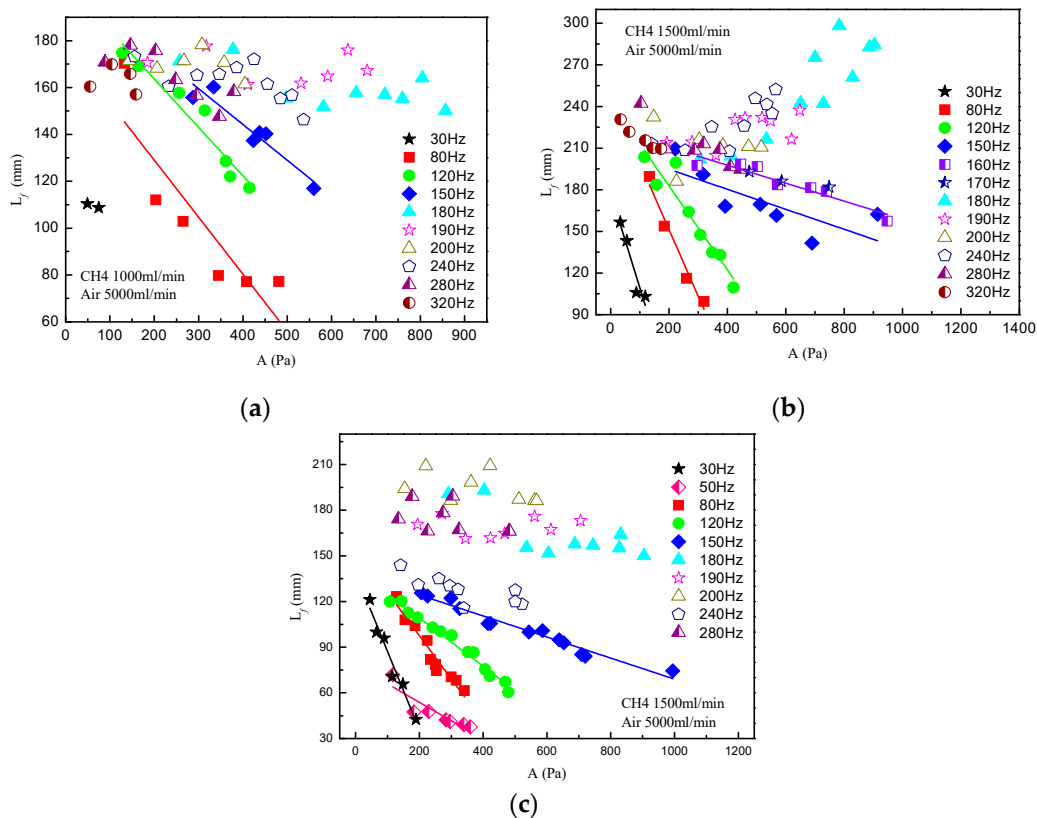

Figure 7. Flame length characteristics with different acoustic parameters; (**a**) Case 1; (**b**) Case 2. (**c**) Case 3.

3.4. Mechanism for Interaction between EINOx and Vortex

To visualize the interaction between flame and vortex, Mie scattering images and velocity fields were obtained by the PIV system to display vortex structure in the partially premixed flame with acoustic parameters of 110 Hz and 321 Pa for case two. In Figure 8, the white circular scattering image indicated that a vortex shape was generated near the exit of the nozzle by acoustic excitation. The vortex grew, left the flame root, and then moved to the downstream zone of the partially premixed

flame, which could be observed from the velocity contour. It was thought that the periodic acoustic excitation enhanced the mixing of fuel and air, and reduced the flame length. Research results showed that when the flame length reduced, the reaction region of NOx shortened, reaction rate strengthened, and NOx emission decreased [23,38].
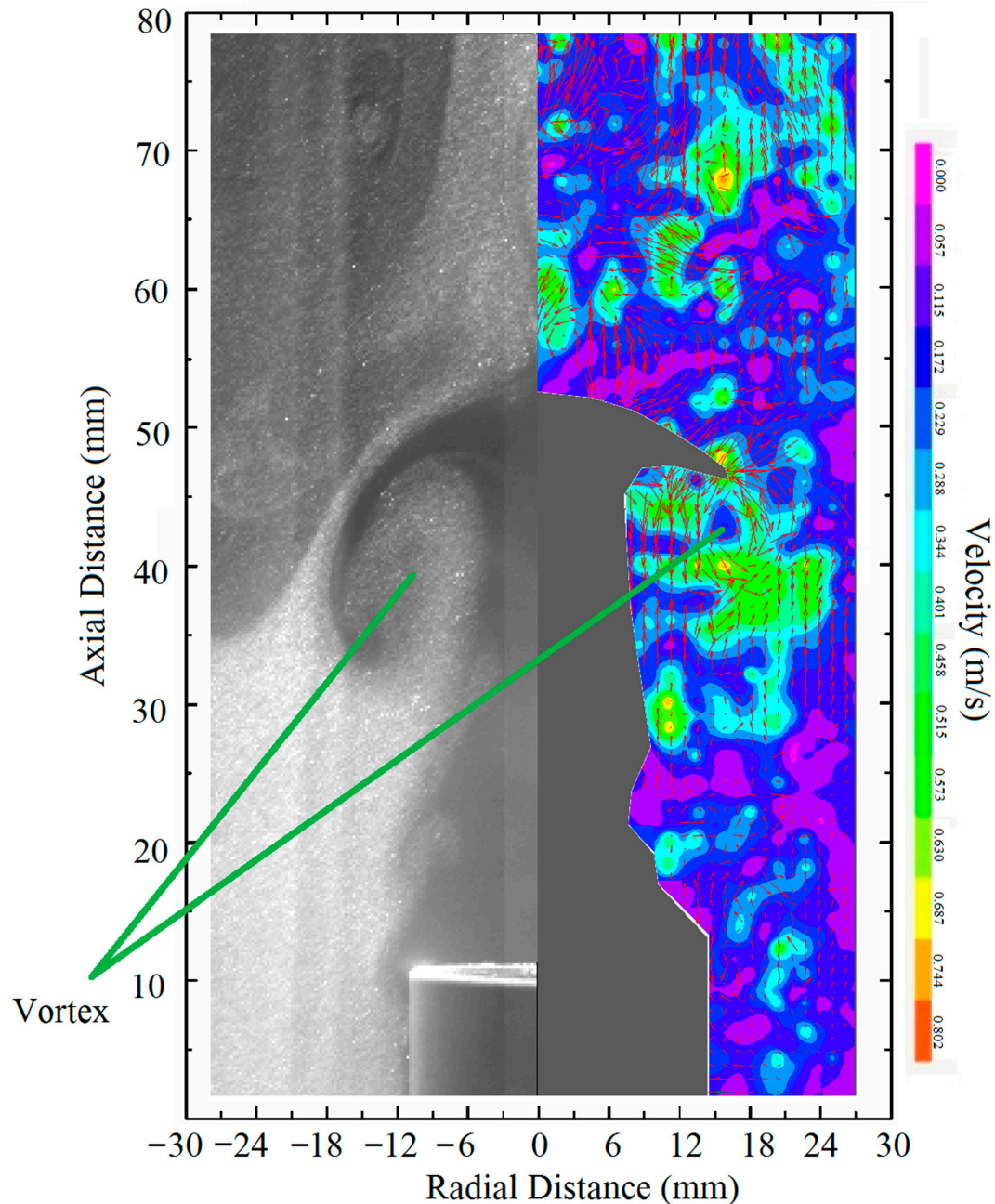
Figure 8. Vortex structure in partially premixed flame under acoustic excitation.

The interaction between vortex and flame was the important mechanism for reduction of NOx in partially premixed flame with acoustic excitation. Figure 9 shows the interaction of flame–vortex under the acoustic frequency range from 80 Hz to 280 Hz in a fixed amplitude at 241 ± 10 Pa. It can be observed that the intensity and position of the vortex showed different characteristics with acoustic frequency. The vortex changed from upstream to downstream with an increase in frequency from 80 Hz to 200 Hz at the same phase. Vortex diameter became larger and the vortex rolled up with surrounding air to the downstream when the acoustic frequency increased. The flame–vortex interaction caused the

flame base to broaden when the frequency was less than f_c (f_c^-), although this broadening effect did not reappear when the frequency was greater than f_c (f_c^+). This corresponded to an increase of NOx emissions induced by the weakness of the mixing effect. This was the reason that EINOx for f_c^- was much less than for f_c^+.
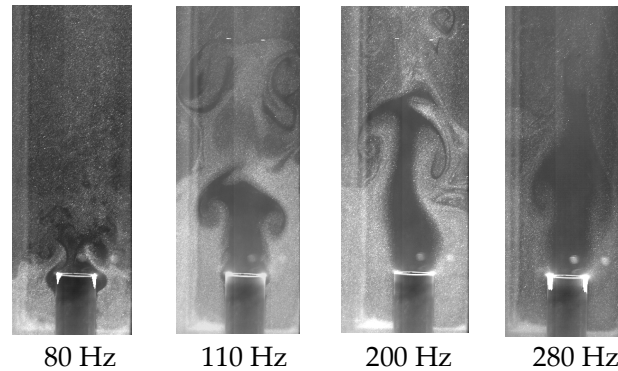

| 80 Hz | 110 Hz | 200 Hz | 280 Hz |

Figure 9. Mie scattering images at different frequency.

As Figure 10 shows, the vortex moved upstream and enhanced the interaction at the base of the flame with an increase of amplitude at 110 Hz, but the influence of amplitude on the length of flame was not obvious at 280 Hz. These changes in flame structure with amplitude variation at different frequencies were well matched with changes of flame length shown in Figure 6. Therefore, NOx emission and flame length both shortened observably with increased acoustic amplitude at 110 Hz; however, it was opposite when the frequency was at 280 Hz.
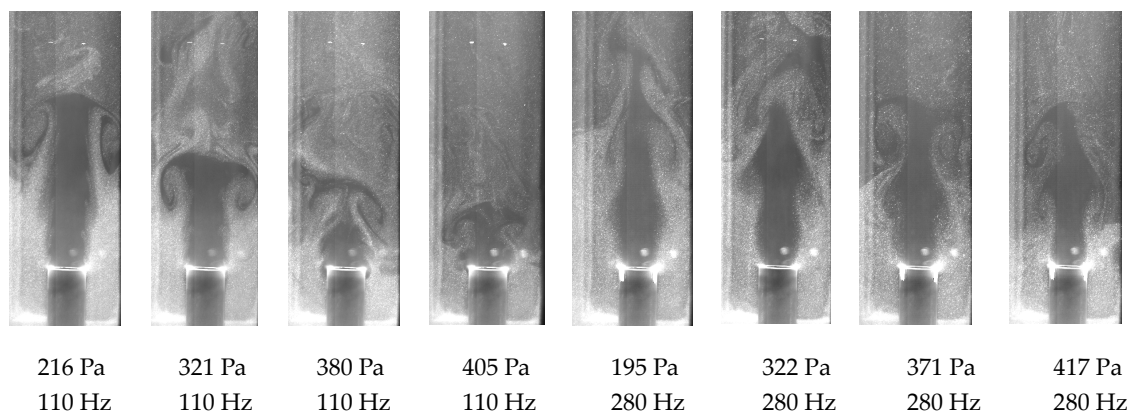

| 216 Pa | 321 Pa | 380 Pa | 405 Pa | 195 Pa | 322 Pa | 371 Pa | 417 Pa |
| 110 Hz | 110 Hz | 110 Hz | 110 Hz | 280 Hz | 280 Hz | 280 Hz | 280 Hz |

Figure 10. Mie scattering images at different acoustic parameters.

4. Conclusions

The NOx emission of partially premixed flames under acoustic parameters of 0–400 Hz/0–1400 Pa were investigated experimentally. The relationship between frequency, amplitude, and EINOx was discussed based on flame length, flame shape, and vortex. The main conclusions are as follows:

(1) The critical frequency f_c, $f_c \in [170, 190]$, occurs in the changing EINOx of partially premixed flame with the increase of amplitude and frequency. A similar phenomenon is also observed in the change of flame length with acoustic parameters. EINOx decreases with the increase of amplitude when $f < f_c$; there is a linear relationship between EINOx and amplitude, and the slope range is from -0.009 to -0.003; EINOx increases with the increase of frequency in a fixed amplitude, and there is also a linear relationship between EINOx and frequency, where the slope range is from 0.01 to 0.03. However, EINOx increases with an increase of amplitude when $f > f_c$, and there is a linear relationship between EINOx and amplitude, where the slope ranges from 0.001 to 0.006.

(2) The flame length decreases with the increase of amplitude when $f < f_c$; the reason is that an increasing acoustic effect makes the flame wrinkle and deform, and the mixing effect of the flow field is enhanced. The flame length increases with the increase of amplitude when $f > f_c$; the reason is that the influence of acoustics on the flame becomes weakened in this frequency range; flame diameter is decreased, and fuel gas velocity is increased with the increase of amplitude. This is the dominant factor for the decrease of EINOx.

(3) Interaction between flame and vortex influences the NOx emission. When acoustic amplitude increases at $f > f_c$, the vortex moves to the upstream zone of the partially premixed flame, there is enhanced interaction at the flame base, and shortened flame length; therefore, NOx emissions decrease.

Author Contributions: Conceptualization, M.W. and Z.S.; methodology, Z.S.; software, Z.S.; validation, M.W., Z.S., and K.D.; formal analysis, M.W.; investigation, Z.S.; resources, K.D.; data curation, M.W. and Z.S.; writing—original draft preparation, M.W. and Z.S.; writing—review and editing, K.D.; visualization, Y.H.; supervision, K.D.; project administration, Y.Z.; funding acquisition, K.D.

Conflicts of Interest: The authors declare no conflict of interest.

References

1. Medwell, P.R.; Nathan, G.J.; Chan, Q.N.; Alwahabi, Z.T.; Dally, B.B. The influence on the soot distribution within a laminar flame of radiation at fluxes of relevance to concentrated solar radiation. *Combust. Flame* **2011**, *158*, 1814–1824. [CrossRef]
2. Wang, C.; Chan, Q.N.; Kook, S.; Hawkes, E.R.; Lee, J.; Medwell, P.R. External irradiation effect on the growth and evolution of in-flame soot species. *Carbon* **2016**, *102*, 161–171. [CrossRef]
3. Chen, C.; Chan, Q.N.; Medwell, P.R.; Yeoh, G.H. Co-combustion characteristics and kinetics of microalgae Chlorella vulgaris and coal through TGA. *Combust. Sci. Technol.* **2018**, 1–20. [CrossRef]
4. Chen, C.; Chen, F.; Cheng, Z.; Chan, Q.N.; Kook, S.; Yeoh, G.H. Emissions characteristics of NOx and SO$_2$ in the combustion of microalgae biomass using a tube furnace. *J. Energy Inst.* **2016**, *90*, 806–812. [CrossRef]
5. Glassman, I.; Yetter, R.A.; Glumac, N.G. *Combustion*, 4th ed.; Academic press: Manhattan, NY, USA, 2014; pp. 154–196.
6. Wang, C.; Wang, P.; Zhao, L.; Du, Y.; Che, D. Experimental Study on NOx Reduction in Oxy-fuel Combustion Using Synthetic Coals with Pyridinic or Pyrrolic Nitrogen. *Appl. Sci.* **2018**, *8*, 2499. [CrossRef]
7. Cho, I.; Lee, Y.; Lee, J. Investigation on the Effects of Internal EGR by Variable Exhaust Valve Actuation with Post Injection on Auto-ignited Combustion and Emission Performance. *Appl. Sci.* **2018**, *8*, 597. [CrossRef]
8. Raun, R.L.; Beckstead, M.W.; Finlinson, J.C.; Brooks, K.P. A review of Rijke tubes, Rijke burners and related devices. *Prog. Energy Combust. Sci.* **1993**, *19*, 313–364. [CrossRef]
9. Rayleigh, J.W.S. The explanation of certain acoustic phenomena. *Nature* **1878**, *18*, 319–321. [CrossRef]
10. Putnam, A.A.; Belles, F.E.; Kentfield, J.A.C. Pulse combustion. *Prog. Energy Combust. Sci.* **1986**, *12*, 43–79. [CrossRef]
11. Zinn, B.T. *Pulsating Combustion*, 4th ed.; Academic press: New York, NY, USA, 1986; pp. 113–181.
12. Drogue, S.; Breininger, S.; Ruiz, R. Minimization of NOx emissions with improved oxy-fuel combustion: Controlled pulsated combustion. *Ceram. Eng. Sci. Proc.* **1994**, *15*, 147–158.
13. McQuay, M.Q.; Dubey, R.K.; Nazeer, W.A. An experimental study on the impact of acoustics and spray quality on the emissions of CO and NO from an ethanol spray flame. *Fuel* **1998**, *77*, 425–435. [CrossRef]
14. Keller, J.O.; Hongo, I. Pulse Combustion—The Mechanisms of NOx Production. *Combust. Flame* **1990**, *80*, 219–237. [CrossRef]
15. Michel, Y.; Belles, F.E. Effects of Flue-Gas Recirculation on NOx Production and Performance of Pulse Combustion Hot-Water Boilers. *Combust. Sci. Technol.* **1993**, *94*, 447–468. [CrossRef]

16. Au-Yeung, H.W.; Garner, C.P.; Hanby, V.I. An experimental study of the effects of combustion frequency and pressure amplitude on the NO emissions from pulse combustors. *J. Inst. Energy* **1998**, *71*, 204–208.

17. Poppe, C.; Sivasegaram, S.; Whitelaw, J.H. Control of NOx emissions in confined flames by oscillations. *Combust. Flame* **1998**, *113*, 13–26. [CrossRef]

18. Hardalupas, Y.; Selbach, A. Imposed oscillations and non-premixed flames. *Prog. Energy Combust. Sci.* **2002**, *28*, 75–104. [CrossRef]

19. Chao, Y.C.; Huang, Y.W.; Wu, D.C. Feasibility of controlling NOx emissions from a jet flame by acoustic excitation. *Combust. Sci. Technol.* **2000**, *158*, 461–484. [CrossRef]

20. Delabroy, O.; Lacas, F.; Poinsot, T.; Candel, S.; Hoffmann, T.; Hermann, J.; Vortmeyer, D. A study of NOx reduction by acoustic excitation in a liquid fueled burner. *Combust. Sci. Technol.* **1996**, *119*, 397–408. [CrossRef]

21. Hassan, M.I.; Wu, T.W.; Saito, K. A combination effect of reburn, post-flame air and acoustic excitation on NOx reduction. *Fuel* **2013**, *108*, 231–237. [CrossRef]

22. Kim, K.T.; Lee, J.G.; Quay, B.D.; Santavicca, D.A. Response of partially premixed flames to acoustic velocity and equivalence ratio perturbations. *Combust. Flame* **2010**, *157*, 1731–1744. [CrossRef]

23. Kim, M.; Choi, Y.; Oh, J.; Yoon, Y. Flame–vortex interaction and mixing behaviors of turbulent non-premixed jet flames under acoustic forcing. *Combust. Flame* **2009**, *156*, 2252–2263. [CrossRef]

24. Chung, D.H.; Lin, T.H.; Hou, S.S. Flame synthesis of carbon nano-onions enhanced by acoustic modulation. *Nanotechnology* **2010**, *21*, 435604. [CrossRef]

25. Kim, K.T.; Hochgreb, S. The nonlinear heat release response of stratified lean-premixed flames to acoustic velocity oscillations. *Combust. Flame* **2011**, *158*, 2482–2499. [CrossRef]

26. Shen, Z.; Deng, K.; Lu, B.; Zhong, Y. Effects of Equivalence Ratio and Velocity on NOx Emissions in Methane Partially Premixed Flames with Acoustic Excitation. *Proc. CSEE* **2013**, *33*, 54–60.

27. Deng, K.; Zhao, Y.; Fang, D.; Zhong, Y. NOx Emission from Methane Jet Diffusion Flames at Different Coaxial Air Flow Rates. *J. Chin. Soc. Power Eng.* **2010**, *11*, 874–882.

28. Deng, K.; Zhong, Y.; Li, H. Experimental study on NOx emission from methane self-excited pulsating combustion. *J. Chin. Soc. Power Eng.* **2010**, *30*, 528–535.

29. Zhong, Y.; Deng, K.; Li, H.; Li, W.; Wu, M. Experimental Study of NOx Emission in Partially Premixed Flame under Acoustic Forcing. *J. Eng. Thermophys.* **2011**, *32*, 1609–1612.

30. Illingworth, S.J.; Waugh, I.C.; Juniper, M.P. Finding thermoacoustic limit cycles for a ducted Burke-Schumann flame. *Proc. Combust. Inst.* **2013**, *34*, 911–920. [CrossRef]

31. Meunier, P.; Costa, M.; Carvalho, M.G. The formation and destruction of NO in turbulent propane diffusion flames. *Fuel* **1998**, *77*, 1705–1714. [CrossRef]

32. Morcos, V.H.; Abdel-Rahim, Y.M. Parametric study of flame length characteristics in straight and swirl light-fuel oil burners. *Fuel* **1999**, *78*, 979–985. [CrossRef]

33. Cheng, T.S.; Chao, Y.C.; Wu, D.C. Effects of partial premixing on pollutant emissions in swirling methane jet flames. *Combust. Flame* **2001**, *125*, 865–878. [CrossRef]

34. Costa, M.; Parente, C.; Santos, A. Nitrogen oxides emissions from buoyancy and momentum controlled turbulent methane jet diffusion flames. *Exp. Therm. Fluid Sci.* **2004**, *28*, 729–734. [CrossRef]

35. Bourehla, A.; Baillot, F. Appearance and Stability of a Laminar Conical Premixed Flame Subjected to an Acoustic Perturbation. *Combust. Flame* **1998**, *114*, 303–318. [CrossRef]

36. Dah-You, M.A.A. Simple theory of Rijke tube oscillation. *Acta Acust.* **2001**, *26*, 289–294.

37. Dah-You, M.A.A. Exact solution of the Rijke tube equation. *Acta Acust.* **2002**, *27*, 288.

38. Oh, J.; Heo, P.; Yoon, Y. Acoustic excitation effect on NOx reduction and flame stability in a lifted non-premixed turbulent hydrogen jet with coaxial air. *Int. J. Hydrogen Energy* **2009**, *34*, 7851–7861. [CrossRef]